American Journal of Environmental Protection, 2025, Vol. 13, No. 1, 16-30
Available online at http://pubs.sciepub.com/env/13/1/3
Published by Science and Education Publishing
DOI:10.12691/env-13-1-3

Land Use/Land Cover Dynamics Effects on Urban Heat Islands: A Case Study of Dakar Region

Noé Valentin Loembet Makaya[1,2,*], Mamadou Lamine Ndiaye[2], Vieux Boukhaly Traore[3], Omar Ngor Thiam[3]

[1]Institut Supérieur d'Informatique (ISI), Dakar, Senegal
[2]Centre de Suivi Ecologique (CSE), Dakar, Senegal
[3]Fluid Mechanics, Hydraulics and Transfers Laboratory, Cheikh Anta Diop University, Dakar, Senegal
*Corresponding author: noemakaya19@gmail.com

Received March 25, 2025; Revised April 28, 2025; Accepted May 05, 2025

Abstract This study aims to analyze the relationship between land use/land cover units and surface temperatures in the Dakar region. Indeed, the concentration of human activities and rapid urbanization have led to an intensification of urban heat islands. This phenomenon influences the city's climate, the rates and distribution of pollutants, the comfort of city dwellers, and the natural elements of cities. Therefore, the effect of urban heat islands is an urban data to be taken into consideration in the design, development and management of the city to create a healthier and more viable environment for the well-being of city dwellers. It is in this context that we initiated a study based on the analysis of land use/land cover dynamics over the period 1986-2023 integrating satellite data and Landsat images. To do this, we first calculated indices such as the surface temperature index (LST), the vegetation index (NDVI), and the built-up area index (NDBI), to quantify the impact of land use/land cover changes on heat islands; we then integrated an urban-rural gradient analysis to assess the variation of environmental parameters according to the distance from urban to rural areas. This provides an in-depth understanding of environmental dynamics and interactions between green spaces and built-up areas.

Keywords: *Land use/Land cover dynamics, land surface temperatures, climatic hazards, NDBI, NDVI, Dakar*

Cite This Article: Noe Valentin Loembet MAKAYA, Mamadou Lamine Ndiaye, Vieux Boukhaly Traore, and Omar Ngor Thiam, "Land Use/Land Cover Dynamics Effects on Urban Heat Islands: Case Study of Dakar Region." *American Journal of Environmental Protection*, vol. 13, no. 1 (2025): 16-30. doi: 10.12691/env-13-1-3.

1. Introduction

The urban heat island effect is a little-known physical climatic phenomenon compared to other manifestations of the same order such as the greenhouse effect responsible for climate change [1,2]. It is generated by the city, its morphology, its materials, its natural, climatic and meteorological conditions, its activities, etc. [3,4]. The urban heat island is characterized by the observation of higher temperatures in an urban area than in its immediate environment [5,6]. This increase is the first manifestation of the city's influence on its site and its natural environment and results from the combination of several factors: geographical and climatic situation, seasons, weather, but also characteristics specific to the city (urbanization model, relief, etc.) [7,8]. This warming of the dense area of the region decreases the relative humidity of the air, because the increase in temperatures limits the pressure of water vapor in the air decreases since there is almost no evaporation [9]. This decrease in the relative humidity of cities in turn leads to a decrease in the number of foggy days and their intensity [3,5]. In addition, the waterproofing of soils in cities is accompanied by the immediate collection of rainwater which is then discharged into watercourses via stormwater networks [10,11]. The heat island finally has effects on the precipitation regime by multiplying stormy episodes or showers because the heat at the city level causes air masses to rise by convection and thus makes the atmosphere unstable [12]. Due to their nature and low albedo. [13,14] argue that construction and development materials absorb solar energy and release it as heat into the atmosphere, thereby creating heat islands in urban areas. According to [15], this profoundly disrupts the living environment and health of residents. In this sense, [16,17] adds that thermal discomfort is one of the recurring problems for city dwellers. The urban heat island effect is therefore an urban fact that must necessarily be taken into consideration in the design and management of the city to offer city dwellers a healthy and sustainable environment [18,19]. However, it is clear that the various urban policies are still far from really taking into account this phenomenon, which requires and will require even more in the future if nothing is done today, a reasoned adaptation of the city [20,21]. At present, the various planning and urban development documents are still relatively unadvanced on the subject, particularly when compared to equivalent foreign documents [22]. According to [23], the analysis of land use/land cover change is an important step towards understanding surface

temperatures. It is a privileged entry point in the assessment of interactions between humans and their environment [24]. According to [12], the information from the study of land use is useful for identifying appropriate strategies to better manage the state of land use. [25,26] used the surface temperature index to show the influence of land use/land cover units on surface temperatures resulting in the creation of urban heat islands and to analyze the evolution of this influence over time. It is in this same vein that this study was initiated in the Dakar region. It is based on satellite data and Landsat images over a period from 1986 to 2023. Several methods have emerged to exploit such data, with varying levels of effectiveness [27]. Among these, diachronic and multi-date analysis of land use/land cover is one of the most widely used because it takes into account the spatial distribution of changes [28,29]. The authors [30,31,32,33] have each successfully used this approach. This is what prompted us to use diachronic and multi-date analysis of land cover in this study. Our approach is essentially based on the calculation of three indices: Land Surface Temperature (LST); Normalized difference vegetation index (NDVI) and Normalized Difference Built-Up Index (NDBI) and on the analysis of the urban-rural gradient. These indices are frequently used in the literature because of their robustness and reliability for such a study [34,35,36]. Our objective through this study is: (i) to study the multi-temporal dynamics of land use/land cover change; (ii) to monitor the dynamics of change and their effect in the Dakar region; (iii) to visualize the role and influence of green spaces on surface temperatures and (iv) to observe the temperature differences between urban and rural areas as well as their mutual influence in the Dakar region. At the end of this study we obtained consistent and revealing results.

2. Study Area

Dakar is one of the 14 regions of Senegal located in the far west of the Cap-Vert peninsula on the Atlantic Ocean. It is located between longitudes 17° 10' and 17° 32' west and latitudes 14° 53' and 14° 35' north [37]. It is bordered to the east by the Thiès region and to the north, west and south by the Atlantic Ocean. Its climate is dry tropical characterized by two seasons, a dry season and a rainy season [38]. The Dakar region is made up of 5 departments: Dakar, Pikine, Rufisque, Guédiawaye and Keur Massar. Its population is estimated at 3,137,196 inhabitants, for an area of 572 km². The Dakar region is also the political and economic capital of Senegal, hence the high concentration of infrastructure and industries [39,40].

3. Data

3.1. Satellite Data

We used satellite data integrating three factors. The first factor relates to the availability of high-resolution images of the Dakar region over a period of approximately 30 years. The second factor relates to the period of image acquisition corresponding to the dry season, particularly the months of March and April, because at this time, there is no cloud cover over the study area and no influence of rain on the vegetation cover either. The third factor relates to the fact that in some scenes, the entire study area is not covered by the sensor, hence the obligation to acquire two images covering the entire area over the same month and to mosaic them.

3.2. Landsat Images

Landsat is a joint program of the National Aeronautics and Space Administration (NASA) and the United States Geological Survey (USGS) for the acquisition of satellite images. These satellites are equipped with sensors that allow them to observe and collect data. Among these sensors, we can cite the RGB (Return Beam Vidicon) sensor, the MSS (Multi Spectral Scanner) sensor, the TM (thematic mapper) sensor, the ETM+ (Enhanced Thematic Mapper Plus) sensor and the OLI_TIRS (Operational Land Imager and Thermal Infrared Sensor) sensor. For this study, we used images acquired with the following sensors: TM (1986-04-30 and 2010-04-16), ETM+ (2000-04-12 and 2000-04-28) and OLI_TIRS (2023-03-10 and 2023-03-11) (Table 1, Table 2) given their popularity and reliability.

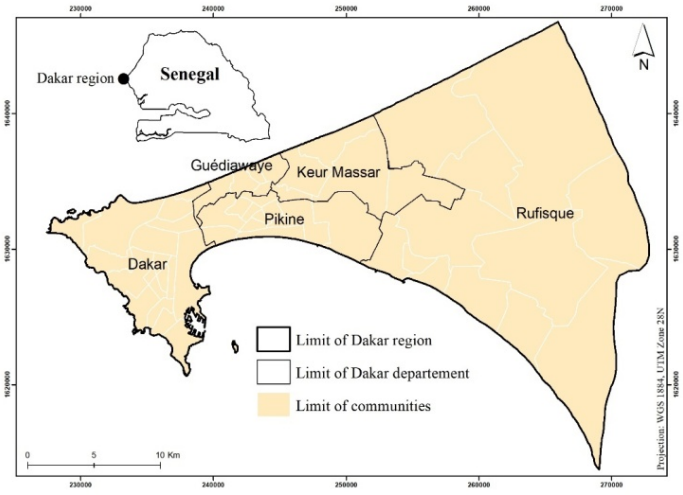

Figure 1. Study Area, Dakar region

Table 1. Landsat datasets of the study area (1986 to 2023)

Satellite	Sensor	Scene ID	Acquisition Date	Time
Landsat 5	TM	LT05_L2SP_205050_19860430_20200918_02_T1	30 April 1986	10 :52 :32
Landsat 7	ETM+	LE07_L2SP_205050_20000412_20200918_02	12 April 2000	11 :19 :46
Landsat 7	ETM+	LE07_L2SP_205050_20000428_20200918_02	28 April 2000	11 :19 :46
Landsat 5	TM	LT05_L1TP_205050_20100416_20200824_02_T1	16 April 2010	11 :18 :21
Landsat 8	OLI_TIRS	LC08_L1TP_206050_20230310_20230320_02_T1	10 March 2023	11 :33 :37
Landsat 9	OLI_TIRS	LC09_L1TP_205050_20230311_20230311_02_T1	11 March 2023	11 :27 :36

Table 2. Landsat 5 TM, Landsat 7 ETM+ and Landsat 8-9 OLI-TIRS sensor characteristics

Satellites	**Landsat 8-9**			**Landsat 7**			**Landsat 5**		
Sensors	Operatinal Land Imager (OLI) and Thermal Infrared Sensor (TIRS)			Enhanced Thematic Mapper Plus (ETM+)			Thematic Mapper (TM)		
Bands Designation	Wavelength	Band	Resolution	Wavelength	Band	Resolution	Wavelength	Band	Resolution
Band 1	0,433-0,453 µm	Coastal/Aerosol	30 m	0,45-0,52 µm	Blue	30 m	0,45-0,52 µm	Blue	30 m
Band 2	0,45-0,515 µm	Blue	30 m	0,53-0,61 µm	Green	30 m	0,52-0,6 µm	Green	30 m
Band 3	0,525-0,6 µm	Green	30 m	0,63-0,69 µm	Red	30 m	0,63-0,69 µm	Red	30 m
Band 4	0,63-0,68 µm	Red	30 m	0,78-0,9 µm	Near Infrared (NIR)	30 m	0,76-0,9 µm	Near Infrared (NIR)	30 m
Band 5	0,845-0,885 µm	Near Infrared (NIR)	30 m	1,55-1,75 µm	Shortwave Infrared (SWIR)	30 m	1,55-1,75 µm	Shortwave Infrared (SWIR)	30 m
Band 6	1,56-1,66 µm	Shortwave Infrared (SWIR 1)	30 m	2,09-2,35 µm	Thermal Infrared (TIR)	60 m (resampled to 30 m)	2,08-2,35 µm	Thermal Infrared (TIR)	120 m (resampled to 30 m)
Band 7	1,36-1,39 µm	Shortwave Infrared (SWIR 2)	30 m	10,4-12,5 µm	Shortwave Infrared (SWIR)	30 m	10,4-12,5 µm	Shortwave Infrared (SWIR)	30 m
Band 8	2,1-2,3 µm	Panchromatic	15 m	0,52-0,9 µm	Panchromatic	15 m			
Band 9	10,3-11,3 µm	Cirrus	30 m						
Band 10	11,5-12,5 µm	Thermal Infrared (TIR 1)	100 m (resampled to 30 m)						
Band 11	0,5-0,68 µm	Thermal Infrared (TIR 2)	100 m (resampled to 30 m)						

4. Material and Method

4.1. Material

To carry out this study, we used Quantum GIS (or Q-GIS) software for data preprocessing and processing. It is a GIS tool that allows vector and raster data to be processed, thanks to the multitude of functions it contains such as the semi-automatic classification plugin that brings together most of the elements necessary for satellite image processing.

4.2. Method

We have subdivided our methodological approach into 4 parts: (i) preprocessing of satellite images, (ii) detection of land cover change, (iii) calculation of vegetation indices (Normalized difference vegetation index) NDVI, Built index (Normalized Difference Built-up Index) NDBI and surface temperature index (LST) and (iv) evaluation of the urban-rural gradient**.**

4.2.1. Pre-treatment

To conduct a study on change detection and index calculation based on pixel processing, it is necessary that the images used have the most homogeneous characteristics possible so that the differences resulting from their comparison are associated with real changes in the state of the territory [41]. In order to counter these shortcomings, the images will undergo a radiometric correction commonly called preprocessing to then make the mosaic of our images from 2000 and 2023 representing the study area in order to then be able to

move on to the different treatments.

√ **Radiometric calibration**

This involves converting the signal recorded by the satellite into a physical variable such as radiance. The recorded values are presented in the form of digital values or digital numbers (DN) corresponding to the digitization of the electrical signal at the sensor output. With the raster calculator tool, they are converted into radiances using the formula (1) [41,43]. In order to normalize the differences in spectral bandwidth by taking into account the spectral distribution of sunlight and to compensate for the influence of solar elevation which varies with the date, time and location, it is necessary to transform the radiances into effective reflectance at the sensor or exo-atmospheric reflectance using equation (2) [44].

$$L = \left(\frac{LMAX - LMIN}{Q_{calmax} - Q_{calmin}} \right) \left(Q_{cal} - Q_{calmin} \right) + LMIN \quad (1)$$

L = radiance in the considered channel

Qcal = numerical value of the image

Qcalmin = minimum radiometric value of the image corresponding to $L_{MIN\lambda}$ (DN)

Qcalmax = maximum radiometric value of the image corresponding to $L_{MAX\lambda}$ (DN)

L_{MIN} = minimum radiance of the channel band to be processed

L_{MAX} = Maximum radiance of the channel band to be processed

$$Pp = \frac{\pi . L_{\lambda} . d^2}{ESUN_{\lambda} . \cos\theta_s} \quad (2)$$

Pp = Effective reflectance at the satellite

π = Mathematical constant equal to approximately 3.14

d = Earth-Sun distance in astronomical units

E_{SUN} = Mean solar exo-atmospheric irradiance

θs = solar elevation angle in degrees

√ **Mosaic Formation**

The images recorded by the sensors form a set of scenes. When all the scenes are grouped together to form an image, we speak of a mosaic. The Dakar region is covered by two scenes in 2000 and 2023. It then becomes necessary to resort to mosaicking to have a global image covering the entire region for each year [41]. For this, we used a QGIS extension called Merge which uses an automatic method based on the connection of georeferenced scenes.

4.2.2. Land Use Land Cover Change Detection

Change detection is the implementation of techniques to highlight the change in land use/land cover in order to understand its temporal evolution [45]. This detection is done by classifying several images of the same scene taken in 1986, 2000, 2010, and 2023. In our study, supervised classification is used, based on familiarity and good knowledge of the study area [46]. To do this, we started with the combination of bands, which consists of gathering all the bands except that of the thermal channel in a single image in order to be able to apply a colored composition. We did the latter by selecting 3 bands from the visible spectrum. For our colored combination, we selected the near infrared corresponding to band 4 for Landsat TM, ETM and corresponding to band 5 for Landsat OLI. Red corresponding to band 3 for Landsat TM, ETM+ and corresponding to band 4 for Landsat OLI. And green corresponding to band 2 Landsat TM, ETM+ and corresponding to band 3 for Landsat OLI. This colored composition is called false color infrared, because it highlights vegetation in red, built-up areas in gray, bare soil in yellow and water in black [11]. The elements mentioned above, vegetation, built-up areas, bare soil, and water will constitute our classes or land use/land cover units [47]; the next step in the classification process is the sampling of classes. For this purpose, for each class we selected a sample of pixels called ROI (Region of Interest) in the form of a polygon subjected to the classification algorithm for each year. For the choice of the classification algorithm, the semi-automatic classification tool in QGIS offers us 3 supervised classification algorithms which are: minimum distance, maximum likelihood, special angle mapping. The maximum likelihood classification algorithm was used in our study because it is based on a statistical analysis of the distribution of the spectral vectors of the sample to define areas of equivalent probability around these centers. The probability of belonging to each class is calculated for each spectral vector assigned to the class for which the probability is the highest. A considerable advantage of this method is that it provides for each pixel, a certainty index linked to this choice [46,48]. After obtaining the classification results, we used the QGIS Boundary clean tool to smooth the irregular edges of the class boundaries and group them together. This operation increases the spatial coherence within the classes. Adjacent regions that belong to the same class can be connected [41]. Accuracy assessment is very important to determine the quality and reliability of results and uncertainty information derived from remote sensing data. It is the procedure used to compare classification results to assumed corrected geographic reference data. It is necessary to pay attention to classification in land use/land cover monitoring, studies using the post-classification comparison method, where the classification error will affect the accuracy of change detection results. Field data, high-resolution images or existing maps are commonly used to assess the quality of classification results produced from any imagery source, to generate an error matrix and accuracy measures for each land use/land cover or land cover map. To assess the accuracy of our classifications, 200 reference plots were selected in the form of polygons on very high-resolution Google Earth images under the supervision of two remote sensing experts, while distributing the 200 reference plots proportionally between the 4 land use/land cover units for each of our images. To assess the accuracy of the user and the producer, an error matrix was applied using the Accuracy tool to compare the relationship between the classified maps and the reference data. The overall accuracy and the Kappa coefficient were used to assess the accuracy of our classifications [49,50]. Finally, for the statistical study of the evolution of land use/land cover, the images obtained were converted into vectors with the Raster to vector tool to merge the different classes and be able to calculate in the attribute table the areas and percentages of land use/land cover of the different classes for each year.

4.2.3. Index Computation

√ **NDVI computation**

The NDVI (Normalized difference vegetation index) is calculated by the raster calculator tool in QGIS software, using the near infrared (NIR) and red (R) bands. Near infrared represents band 4 for Landsat TM (0.76-0.90 µm), band 4 for Landsat ETM+ (0.75 - 0.90 µm) and band 5 for Landsat OLI (0.845-0.885 µm). Red represents band 3 for Landsat TM (0.63-0.69 µm), for Landsat ETM+ (0.63 - 0.69 µm) and band 4 for Landsat OLI (0.630-0.680 µm), respectively. The NDVI index provides a very accurate picture of the vegetation at a given time. It is derived from the difference between the reflectance of vegetation provided by the near infrared and the red, divided by their sum translated by equation (3) [51].

$$NDVI = \frac{NIR - R}{NIR + R} \quad (3)$$

The NDVI index takes the form of a new image, the value of each pixel being between -1 (bare ground) and 1 (maximum plant cover) [50]. It is the analysis of the range of nuances extending between these extreme values (very infrequent) that will inform the observer about the density of cover and the quantity of green biomass. This index is widely used for monitoring plant cover because of the ease of its implementation and especially its correlation with the density of plant cover and the capacity of plants to absorb sunlight) [52].

√ **NDBI computation**

The NDBI Normalized Difference Built-up Index uses the near infrared (NIR) and short wavelength infrared (SWIR) bands to highlight built-up areas. For Landsat TM, the near infrared is represented by band 4 and short wavelength infrared by band 5. For Landsat ETM+, the near infrared is represented by band 4 and short wavelength infrared by band 5. As for Landsat OLI, the near infrared is represented by band 5 and short wavelength infrared by band 6. The calculation was carried out by the raster calculator tool, applying equation (4) allows to obtain a new NDBI image whose pixel values are between -1 and 1 [53].

$$NDBI = \frac{SWIR - NIR}{SWIR + NIR} \quad (4)$$

√ **LST computation**

The LST (land surface temperature) index measures the thermal radiation emission of the Earth's surface using the thermal channel of the Landsat sensors, represented by band 6 for Landsat TM, band 6 for Landsat ETM+ and for Landsat OLI the thermal channel has two bands, band 10 and band 11. With the raster calculator tool we start by calculating the spectral radiance (equation 5) which is then converted into brightness temperature (equation 6) which represents the surface temperatures in degrees Kelvin so for the conversion from degrees Kelvin to degrees Celsius, we subtract the value of 273.15 from the result obtained. These two equations are applied to all images to have at the output images whose pixel values are between the maximum and minimum value of the surface temperatures [50].

$$L\lambda = M_L * Q_{cal} + A_L \quad (5)$$

$$TB = \frac{K_2}{LN\left(\frac{K_1}{L_\lambda}\right) + 1} - 273.15 \quad (6)$$

Lλ: spectral radiance,

M_L radiance_multi_Band from the metadata.

Qcal: quantified and calibrated value of the pixels of the standard product (Thermal Band).

A_L radiance_add_Band from the metadata,

T_B brightness temperature,

K1 and K2: thermal conversion constants also from the metadata.

These metadata are contained in a text file downloaded by default when acquiring a satellite image [50,51].

4.2.4. Urban–Rural Gradient

Gradient analysis is a useful method to assess the spatial and temporal variation of environmental variables with distance from the city to the rural area. This analysis provides information about the spatial structure of the average LST, NDVI, and NDBI indices based on the urban-rural gradient. The gradient gives us ideas about the distribution of the different indices and how they fluctuate in the city landscape [29,51].

This task was carried out by taking a sample of the NDVI, NDBI, and LST index values from the city center to its periphery at intervals of 1 km up to 40 km as a point and then generating graphs and analyzing them.

5. Results and Discussions

5.1. Accuracy Assessment Report of LU/LC Classification

The classification of land use/land cover in the Dakar region in 1998, 2000, 2010 and 2023 was carried out on the basis of the 4 land use/land cover classes which are built-up areas, water, vegetation and bare soil (Table 3). These classes were used to classify the images in order to spatialize and represent the land use/land cover dynamics for the 4 years. The overall accuracy obtained for each of the classifications is greater than 90%, 97.6% for 1986, 95.8% for 2000, 97.2% for 2010 and 98.96% in 2023. The Kappa coefficient is 0.921 for 1986, 0.907 for 2000, 0.947 for 2010 and 0.982 for 2023 (Table 4).

Table 3. Delineated classes of land use/land cover (LU/LC) of Dakar region

LU/LC Classes	Description
Impervious Land	Residential, commercial, industrial settlements, parking lots, and transportation
Vegetation Land	Urban vegetation, forest, garden, cultivation plot
Water Bodies	Lake, reservoirs, stormwater, retention basin
Open Land	Bare ground, Runway, Beach, Dune

Table 4. Report of accuracy assessment on LU/LC classification (1986–2023) of Dakar region

LU/LC Classes		Years			
		1986	2000	2010	2023
User Accuracy	Impervious Land	98.6	97.4	96.3	99.7
	Water Bodies	100.0	100.0	100.0	100.0
	Vegetation Land	78.4	96.5	98.6	99.6
	Open Land	99.1	95.2	97.2	98.3
Producer Accuracy	Impervious Land	97.8	85.5	92.3	97.6
	Water Bodies	79.7	90.9	89.01	100.0
	Vegetation Land	92.6	95.7	100.0	98.6
	Open Land	98.1	98.9	98.7	99.8
Overall Accuracy		97.6	95.8	97.2	98.96
Kappa Coefficient		0.921	0.907	0.947	0.982

5.2. Spatiotemporal Pattern of LU/LC Dynamics

Figure 2 represents the land use/land cover map showing the evolution of the different classes over the years. Built-up areas are the class that have expanded the most, increasing from an area of 56.80 km² in 1986 to 100.60 km² in 2000, then 129.30 km² in 2010 and 175.34 km² in 2023 (Table 5 and Figure 3), which represents an increase of 8.87% (or 43.8 km²) between 1986 and 2000, then an increase of 5.12% (or 28.7 km²) between 2000 and 2010, ending with an increase of 8.17% (or 46.04 km²) between 2010 and 2023 (Table 6 and Figure 4). Water is the third class to have expanded, increasing from an area of 56.80 km² in 1986 to 100.60 km² in 2000, then 129.30 km² in 2010 and 175.34 km² in 2023 (Table 5 and Figure 3). 1986 to 100.60 km² in 2000 then 129.30 km² in 2010 and 175.34 km² in 2023 (Table 5 and Figure 3), which is an increase of 0.11% or 0.63 km² between 1986 and 2000 then an increase of 0.04% or 0.22 km² between 2000 and 2010 to finish with an increase of 0.77% or 4.34 km² between 2010 and 2023 (Table 6 and Figure 4). Vegetation is the second class to have expanded the most, increasing from an area of 56.80 km² in 1986 to 100.60 km² in 2000, then 129.30 km² in 2010 and 175.34 km² in 2023 (Table 5 and Figure 3), which is an increase of 2.28% or 12.6 km² between 1986 and 2000, then an increase of 2.4% or 13.45 km² between 2000 and 2010, ending with an increase of 0.1% or 0.67 km² between 2010 and 2023 (Table 6 and Figure 4). Bare soil is the only one of the 4 land use/land cover classes to have declined to the detriment of the others, going from an area of 56.80 km² in 1986 to 100.60 km² in 2000 then 129.30 km² in 2010 and 175.34 km² in 2023 (Table 5 and Figure 3), which is a decrease of -10.26% or -58 km² between 1986 and 2000 then a decrease of -7.55% or -42.07 km² between 2000 and 2010 to finish with a decrease of -9.04% or -50.03 km² between 2010 and 2023 (Table 6 and Figure 4). The total area of the study area increased from 561.18 km² in 1986, 559.31 km² in 2000, 559.61 km² in 2010 and 560.63 km² in 2023 with an average area of 560.18 km² (Table 5). In 1986 in the department of Dakar, there was a strong presence of buildings, ranging from the commune of Plateau to Grand Yoff. Buildings also occupied part of the communes of Ouakam, Ngor, Yoff, and Parcelle assainies. Vegetation is mainly found at the Hann park, in the commune of Patte D'oie, at Plateau, at Fann/Point E/Amitié and at the end of the tip of Almadies. Buildings are found on the border between the departments of Keur Massar, Pikine and Guédiawaye. Filao trees are found all along the coast from Rufisque to Guédiawaye and there is also the classified forest of Mbao in Pikine. In the department of Rufisque, there is building on the border between the communes of Rufisque West, Rufisque Center, and Rufisque East. There are also plots of cultivation distributed in the different communes of Rufisque as well as the pink lake in the commune of Tivaouane Peulh-Niagha. In 2000, there was an expansion of building from west to east, which is due to the construction of infrastructure and housing to meet the needs of the population, the population which is becoming larger and larger. Buildings therefore occupy almost all of the departments of Dakar and Guédiawaye. We observe the presence of Lake Wouye in the department of Keur Massar, a lake on which we observed years ago a tendency to regression, this one due to the drought recorded between 1968 and the end of the 1990s [55]. In the department of Rufisque, we observe the increase in the number of cultivated plots, Rufisque will therefore become the department with the majority of agricultural land in the Dakar region. In 2010, we observe the expansion of the built-up area, which this time occupies almost all of the departments of Pikine and Keur Massar, we also note the expansion of the built-up area in the municipalities of Rufisque West, Rufisque Center, and Rufisque East. Still in Rufisque, we find again an increase in cultivated plots. In 2023, the built-up area continues its expansion this time in the department of Pikine and we also observe the presence of the different water points in the Dakar region.

5.3. Spatiotemporal Pattern of LST Dynamics

Figure 5 shows the dynamics of temperature evolution during the years 1986, 2000, 2010, 2023. We note that the highest temperatures are observed in the east of the Dakar region. In 1986 the temperatures range from 39.2 °C to 45.5 °C, it is a very hot year with an average of 47.34 °C, in 2000 the temperatures range from 14.3 °C to 50.7 °C with an average of 39.20 °C, in 2010 the temperatures range from 15.6 °C to 33.2 °C with an average of 28.63 °C and in 2023 the temperatures range from 18.4 °C to 48.8 °C with an average of 37.07 °C, which means that

between 1986 and 2000 the average temperature dropped by -8 °C, then between 2000 and 2010 it dropped again by -10.57 °C and between 2010 and 2023 the average temperature increased by 8.44 °C. Which places 1986 as the year with the highest temperatures and 2010 as the year with the lowest temperatures (Table 7).

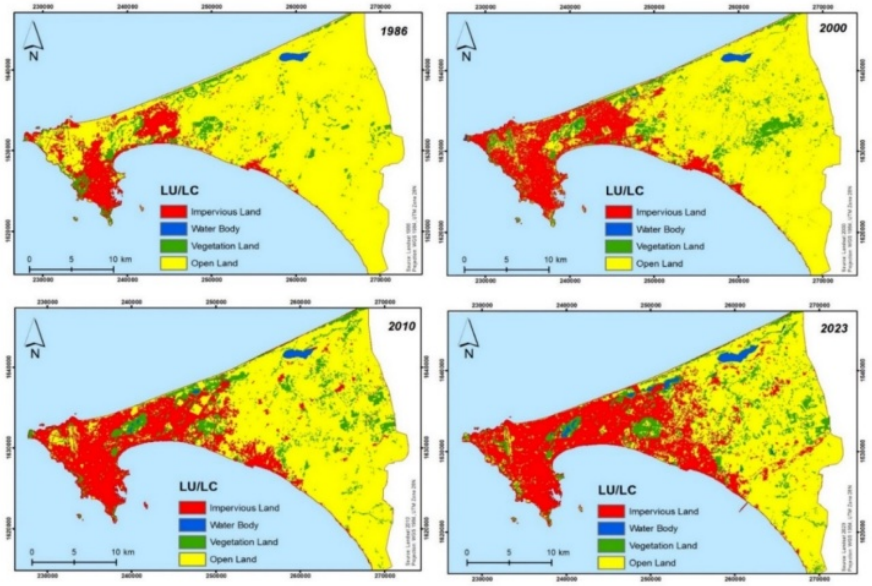

Figure 2. Land use Land cover dynamics in Dakar region between 1986 and 2023

Table 5. LU/LC statistics summary for Dakar region

LU/LC Classes	1986		2000		2010		2023	
	km²	%	km²	%	km²	%	km²	%
Impervious Land	56.80	10.12	100.60	17.99	129.30	23.11	175.34	31.28
Water Bodies	2.95	0.53	3.58	0.64	3.80	0.68	8.14	1.45
Vegetation Land	38.80	6.91	51.40	9.19	64.85	11.59	65.52	11.69
Open Land	462.63	82.44	403.73	72.18	361.66	64.63	311.63	55.59
Total	561.18	100	559.31	100	559.61	100	560.63	100

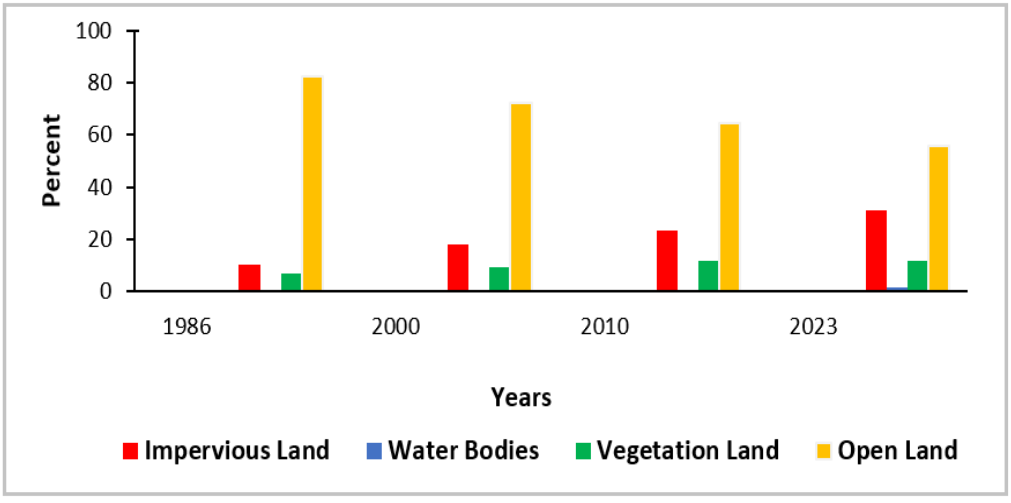

Figure 3. Description of LU/LC statistics of Dakar region

Table 6. LU/LC change statistics for Dakar region

LU/LC Classes	1986-2000		2000-2010		2010-2023	
	km²	%	km²	%	km²	%
Impervious Land	43.8	7.87	28.7	5.12	46.04	8.17
Water Bodies	0.63	0.11	0.22	0.04	4.34	0.77
Vegetation Land	12.6	2.28	13.45	2.4	0.67	0.1
Open Land	-58.9	-10.26	-42.07	-7.55	-50.03	-9.04

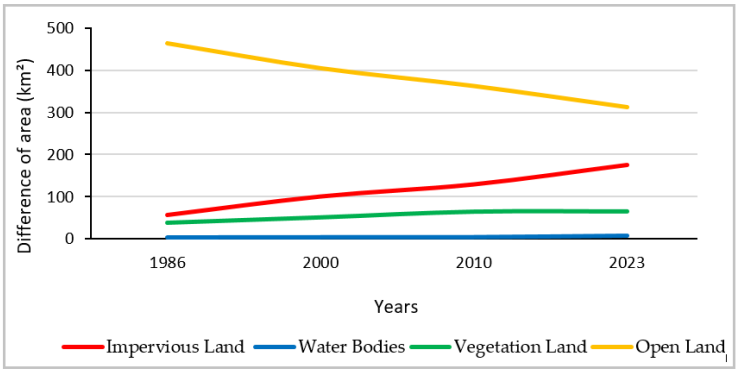

Figure 4. Descriptions of LU/LC class at different time periods in Dakar region

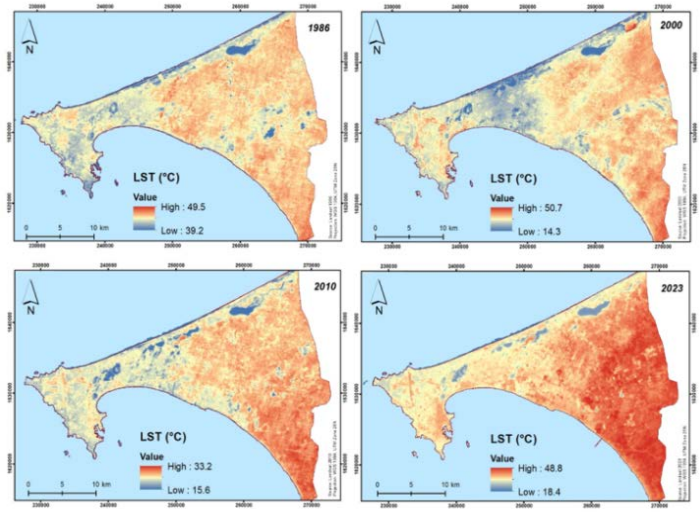

Figure 5. Spatial land surface temperature (LST) dynamics in Dakar region

Table 7. Retrieved statistics of LST values in Dakar region (1986-2023)

Region	Years	Minimum (°C)	Maximum (°C)	Mean (°C)	Standard Deviation (°C)
Dakar	1986	39.22	49.51	47.34	0.75
	2000	14.30	50.74	39.20	3.47
	2010	15.62	33.20	28.63	2.09
	2023	18.46	48.87	37.07	4.31
The difference of Mean LST in Different Time Periods (°C)					
1986-2000		2000-2010		2010-2023	
-8.14		-10.57		8.44	

5.4. LU/LC Effects on LST

To analyze the effect of land use/land cover dynamics on surface temperatures, we used the average temperatures at each class for the years 1986, 2000, 2010 and 2023. At the built-up area level, the average temperature was 47.10°C in 1986, then it fell to 37.37°C in 2000, then fell again to 27.30°C in 2010 and then rose again to 34.38 °C in 2023. This gives a drop of -9.73°C between 1986 and 2000, a drop of -10 °C between 2000 and 2010 and an increase of 7.08 °C between 2010 and 2023. The average water temperature was 45.51°C in 1986, then it drops to 25.98°C in 2000, then drops again to 21.97°C in 2010, then rises again to 25.41°C in 2023. This gives a drop of -18.53°C between 1986 and 2000, a drop of -4.01°C between 2000 and 2010 and an increase of 3.44°C between 2010 and 2023. The average temperature of vegetation was 47.17°C in 1986, then drops to 36.31°C in 2000, then drops again to 26.51°C in 2010, then rises again to 34.97 °C in 2023. This gives a drop of -10.86°C between 1986 and 2000, a drop of -9.8°C between 2000 and 2010 and an increase of 8.46°C between 2010 and 2023. The average temperature of bare soil was 47.56°C in 1986, then it drops to 40.13°C in 2000, then drops again to 29.59°C in 2010, then rises again to 39.33°C in 2023. This gives a decrease of -7.43 °C between 1986 and 2000, a decrease of -10.54°C between 2000 and 2010 and an increase of 9.74°C between 2010 and 2023 (Table 8). A trend is observed, at the level of each year, we find the lowest temperature values at the level of water points then at the level of vegetation while the highest values are observed at the level of bare ground then at the level of buildings (Table 8). The analysis of Table 9 and Figure 6 showed that bare ground is the occupation unit with the highest temperatures. Buildings are the land occupation unit that had the greatest expansion between 1986 and 2023, buildings are also the second occupation unit with the highest temperatures. Its average temperature will be taken as a reference to calculate the difference compared to the average temperature of each of the other occupation units. This will make it possible to observe the difference between the temperature averages corresponding to the nights of land occupation and their changes over the years. Thus the difference between the average temperature of the building and that of the water is 1.59°C in 1986, 11.39°C in 2000, 5.33°C in 2010, 8.97°C in 2023. We note that the temperature differences are positive for the four years; which demonstrates that over these 4 years the average temperatures at the water level are lower than the average temperatures at the building level. The difference between the average temperature of the building and that of the vegetation is -0.07°C in 1986, 1.06°C in 2000, 0.79°C in 2010, -0.59°C in 2023. We note that in 2 of the 4 years the temperature differences are negative values, this is the case in 1986 and 2023, which means that in these 2 years the average temperatures at the vegetation level are higher than the average temperatures at the building level. The difference between the average temperature of the building and that of the bare ground is -0.46°C in 1986, -2.76°C in 2000, -2.29°C in 2010, -4.94°C in 2023. We note that the temperature differences are negative values for the four years which demonstrates that over these 4 years the average temperatures at the level of the bare ground are higher than the average temperatures at the level of the building.

5.5. Spatiotemporal Pattern of NDVI Dynamics and Its Relationship with LST

Figure 7 relates to the vegetation index map showing the dynamics of the evolution of the vegetation cover over the years: 1986, 2000, 2010, 2023. In 1986, the NDVI index values range from 0.28 to -0.15 with an average of 0.08. In 2000, the NDVI index values range from 0.69 to -0.14 with an average of 0.39, this average is the highest. In 2010, the NDVI index values range from 0.52 to -0.41 with an average of 0.02, this average is the lowest. In 2023, the NDVI index values range from 0.57 to -0.28 with an average of 0.13 (Table 10). The lowest NDVI values are observed at water points and inhabited areas, while high NDVI values are found in vegetation zones. Over the 4 years 1986, 2000, 2010 and 2023, dense vegetation is mainly found around watercourses, in the Mbao classified forest, the Hann park, the Technopole and also in the crop plots located in the Rufisque department (Figure 7). Then, to get an overall idea of the quality of the linear adjustment, we graphically exploited 500 points containing the values of the LST and NDVI indices to calculate the coefficient of determination R2. To have a strong correlation, the value of the coefficient of determination R2 must be greater than or equal to 0.5 [55]. In our case, our correlations are all weak because the value of R2 is less than 0.5 for each of the years. R2 corresponds to 0.0 for 1986, R2 corresponds to 0.2 for 2000, R2 corresponds to 0.07 for 2010 and R2 corresponds to 0.1 for 2023. It is noted that the higher the temperature values, the higher the NDVI values, which is explained by the fact that the high density of vegetation has an impact on temperatures, hence the low temperatures in areas of high vegetation density; on the other hand, in areas of non-dense vegetation (herbaceous vegetation), high temperatures are observed as on bare ground and inhabited areas (Figure 5, Figure 7).

5.6. Spatiotemporal Pattern of NDBI Dynamics and its Relationship with LST

The results obtained by calculating the NDBI index for the years 1986, 2000, 2010 and 2023 showed a confusion between built-up areas and bare soil areas. In this study, the NDBI index highlights built-up areas and bare soil areas while originally this NDBI index is supposed to highlight built-up areas. To understand this phenomenon, there are studies in the literature that discuss the interferences between NDBI (built-up index) values and bare soil. This phenomenon is mainly due to the fact that bare soil, especially in arid or semi-arid areas, sometimes shares similar spectral signatures with built-up areas, leading to confusion in the interpretation of NDBI results [14,56]. In this context, we present in Figure 9 the building index map showing the dynamics of the evolution of the building over the years: 1986, 2000, 2010, 2023. In 1986, the values of the NDBI index range from 0.53 to -0.29 with an average of 0.10. In 2000, the values

of the NDBI index range from 0.64 to -0.37 with an average of 0.53, this average is the highest. In 2010, the values of the NDBI index range from 0.49 to -0.42 with an average of 0.31. In 2023, the values of the NDBI index range from 0.33 to -0.37 with an average of 0.31, this average is the lowest (Table 13). Very low NDBI values are observed at the level of dense vegetation and watercourses tendit which the highest NDBI values are observed at the level of bare soil and then at the level of inhabited areas (Figure 9). Then, 500 points containing the values of the LST and NDBI indices were graphically exploited to determine the coefficient of determination R2 in order to have an overall idea of the quality of the linear adjustment. Thus over the 4 years, 3 have a strong correlation: this is the case in 1986 with R2 = 0.6, 2000 with R2 = 0.5, 2010 with R2 = 0.6 but for 2023 the correlation is weak because R2 = 0.4. A trend is observed, the higher the temperature values, the higher the NDBI values (Figure 10).

Table 8. The mean LST over each distinct LU/LC classes in Dakar region from 1986 to 2023

LU/LC	Means LST (°C)				The difference of means LST (°C)		
	1986	2000	2010	2023	1986-2000	2000-2010	2010-2023
Impervious Land	47.10	37.37	27.30	34.38	-9.73	-10	7.08
Water Bodies	45.51	25.98	21.97	25.41	-18.53	-4.01	3.44
Vegetation Land	47.17	36.31	26.51	34.97	-10.86	-9.8	8.46
Open Land	47.56	40.13	29.59	39.33	-7.43	-10.54	9.74

Table 9. The magnitude of mean LST over each distinct LU/LC class in Dakar region from 1986 to 2023

LU/LC	Magnitude of means LST (°C)			
	1986	2000	2010	2023
Impervious Land - Water Bodies	1.59	11.39	5.33	8.97
Impervious Land - Vegetation Land	-0.07	1.06	0.79	-0.59
Impervious Land - Open Land	-0.46	-2.76	-2.29	-4.95

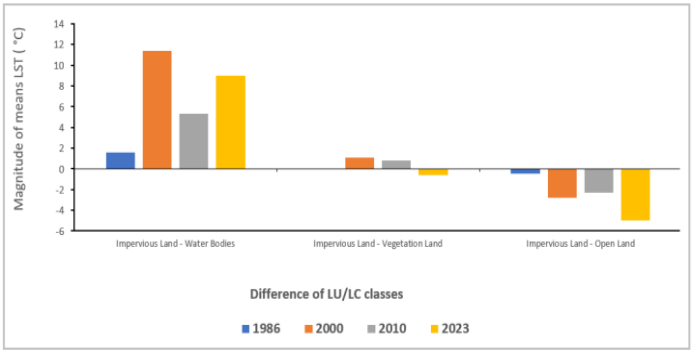

Figure 6. Description of the magnitude of mean LST over each distinct LU/LC class in Dakar region from 1986 to 2023

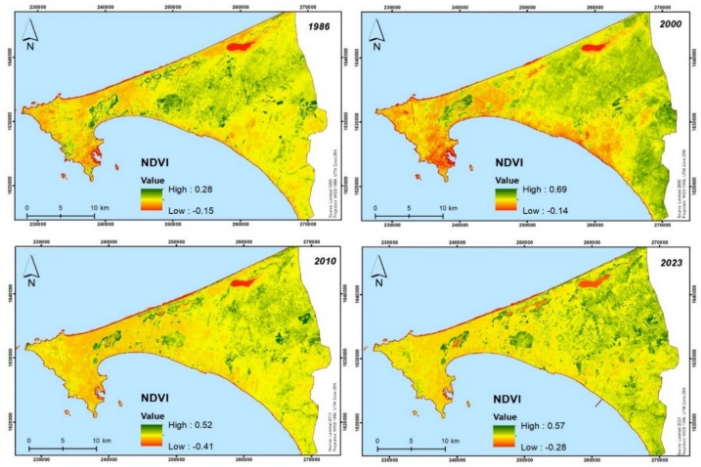

Figure 7. Spatial normal difference vegetation index (NDVI) dynamics in Dakar region

Table 10. Retrieved statistics of NDVI values in Dakar region

Region	Years	Minimum	Maximum	Mean	Standard Deviation
Dakar	1986	-0.15	0.28	0.08	0.02
	2000	-0.14	0.69	0.39	0.05
	2010	-0.41	0.52	0.02	0.06
	2023	-0.28	0.57	0.13	0.06

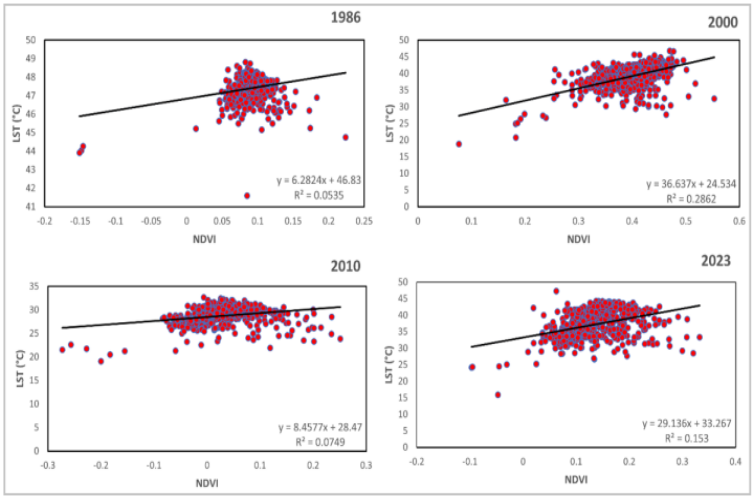

Figure 8. Spatial scattered plots between LST and NDVI in Dakar region

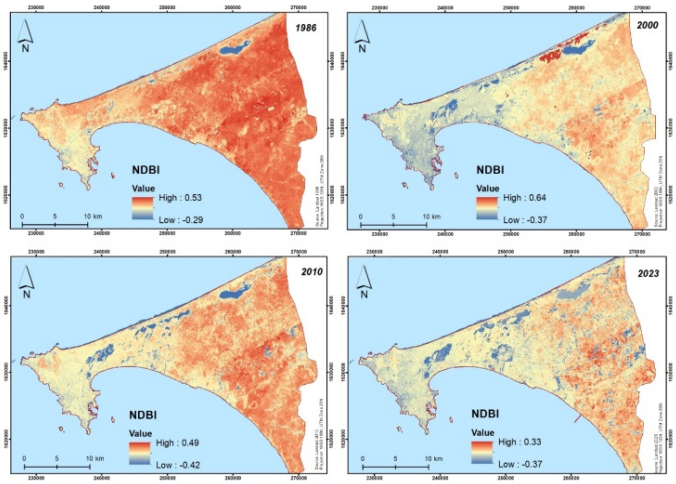

Figure 9. Spatial NDBI dynamics in Dakar region

Table 11. Retrieved statistics of NDBI values in Dakar region

Region	Years	Minimum	Maximum	Mean	Standard Daviation
Dakar	1986	-0.29	0.53	0.10	0.04
	2000	-0.37	0.64	0.53	0.07
	2010	-0.42	0.49	0.31	0.08
	2023	-0.37	0.33	0.06	0.06

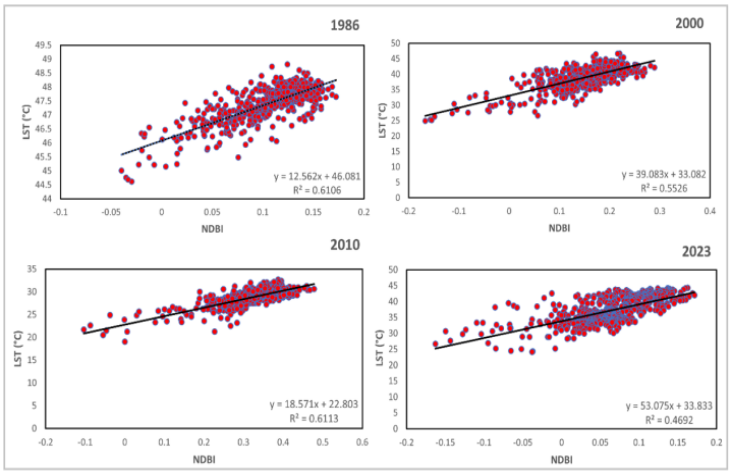

Figure 10. Spatial scattered plots between LST and NDBI in Dakar region.

5.7. Analysis of Patern of Urban Rural Gradient

The three indices LST, NDVI and NDBI were represented on the 40 points going from the department of Dakar to the end of the department of Rufisque over 40 km with a 1 km gap between the points, this for the 4 years: 1986, 2000, 2010 and 2023 (Figure 11). In 1986 in the city center, the average LST was 43.9 °C, the average NDVI was 0.05 and the average NDBI was 0.06. At 32 km from the city center, the average LST goes from 43.9 °C to 47.7 °C, the average NDVI goes from 0.05 to -0.14 and the average NDBI goes from 0.06 to -0.09. After 32 km, we observe the increase in the average LST NDVI and NDBI, the average LST goes from 47.7 °C to 48.3 °C, the average NDVI goes from -0.14 to 0.09, the average NDBI goes from -0.09 to 0.14. In 2000 in the city center, the average LST was 35.6 °C, the average NDVI was 0.34 and the average NDBI was 0.06. At 32 km from the city center, the average LST goes from 35.6 °C to 25.9 °C, the average NDVI goes from 0.34 to 0.17 and the average NDBI goes from 0.06 to -0.14. After 32 km, the average LST, NDVI and NDBI increase, the average LST increases from 25.9 °C to 41.9 °C, the average NDVI increases from 0.17 to 0.45 and the average NDBI increases from -0.14 to 0.22. In 2010 in the city centre, the average LST was 26.3 °C, the average NDVI was 0.04 and the average NDBI was 0.19. At 32 km from the city centre, the average LST increases from 26.3 °C to 21.5 °C, the average NDVI increases from 0.04 to -0.25 and the average NDBI increases from 0.19 to -0.07. After 32 km, we observe the increase in the average of LST, NDVI and NDBI, the average of LST goes from 21.5 °C to 29.1 °C, the average of NDVI goes from -0.25 to 0.01 and the average of NDBI goes from -0.07 to 0.41. In 2023 in the city center, the average of LST was 32.5 °C, the average of NDVI was 0.13 and the average of NDBI was -0.03. At 32 km from the city center, the LST average increases from 32.5 °C to 24.5 °C, the NDVI average increases from 0.13 to -0.09 and the NDBI average remains at -0.03. After 32 km, the increase in the LST, NDVI and NDBI averages is observed, the LST average increases from 24.5 °C to 39.4 °C, the NDVI average increases from -0.09 to 0.14 and the NDBI average increases from -0.03 to 0.12 (Figure 12). For all years, we note that the average of LST, NDVI and NDBI are low at 32 km from the city center except for 1986 where we observe the average of LST is higher than in the city center and for 2023 where we observe the lowest average of NDBI at 23 km from the city center. Then between 32 km and 40 km, we observe an increase in the average of LST, NDVI and NDBI. These different variations can be justified by the influence of land use/land cover on the average of the values of the different indices. The presence of buildings in the city center explains the fairly high average temperature over the 4 years. At 32 km from the city center, we observe a drop in the average LST NDVI and NDBI which is due to the presence of the Lac Rose which is a water point and finally between 32 km and 40 km, we observe a strong presence of bare soil in this part of the department of Rufisque which explains the increase in the average LST. We observe a trend between NDVI and LST, when the average value of NDVI increases the average value of LST decreases and when the average value of NDVI decreases the average value of LST increases. We also observe a trend between NDBI and LST, when the average value of NDBI increases, the average value of LST also increases and when the average value of NDBI decreases the average value of LST also decreases. We can therefore say that vegetation promotes the decrease in surface temperatures while buildings and bare soil promote the increase in surface temperatures (Figure 12).

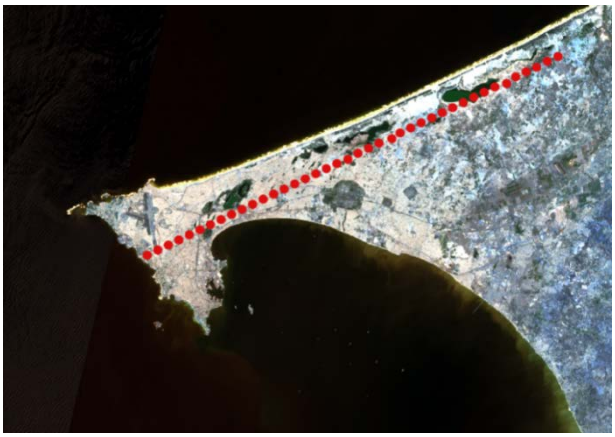

Figure 11. Illustration of collection points for Urban Rural Gradient

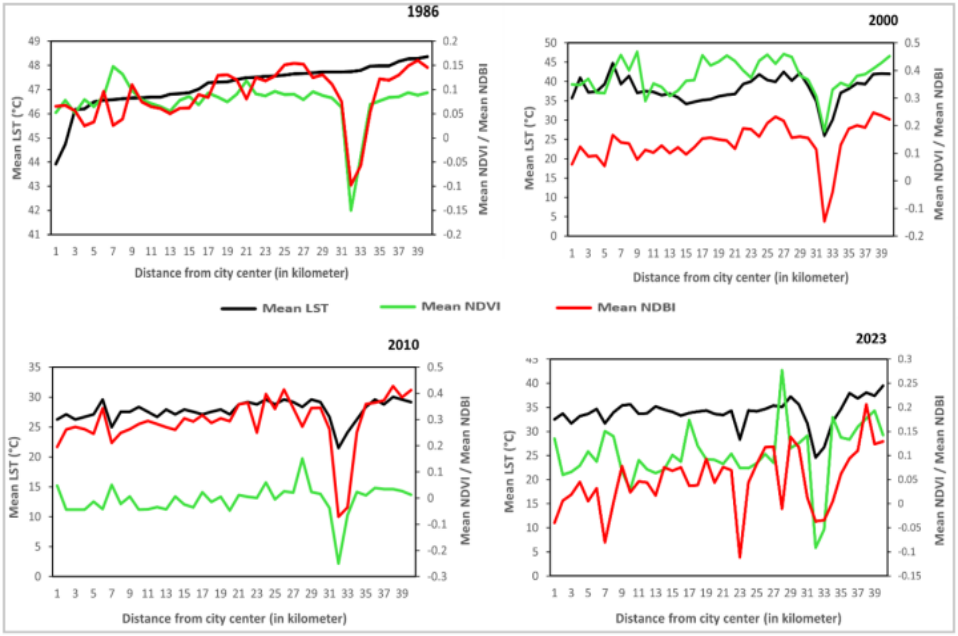

Figure 12. Spatial distribution of urban–rural gradient of LST, NDVI, and NDBI in Dakar region (1986-2023)

6. Conclusions

This study aims to quantify the evolution of land use/land cover change in the Dakar region during the years: 1986, 2000, 2010 and 2023. To achieve this objective, we proceeded with a diachronic and multi-date analysis of land use/land cover. It is based on the calculation of: Land Surface Temperature (LST); Normalized difference vegetation index (NDVI) and Normalized Difference Built-Up Index (NDBI) and on the exploitation of the urban-rural gradient. Our motivation through this study is: (i) to study the multi-temporal dynamics of land use/land cover change; (ii) to monitor the dynamics of change and their effect in the Dakar region; (iii) to visualize the role and influence of green spaces on surface temperatures and (iv) to observe the temperature differences between urban and rural areas as well as their mutual influence in the Dakar region. Thus, at the end of this study we obtained consistent and revealing results. Concerning land use/land cover, the results showed that the area occupied by buildings increased by 118 km² or 21.04% of the total area of the study area, the area occupied by water increased by 5.23 km² or 0.93% of the total area, the area occupied by vegetation increased by 26.72 km² or 4.76% of the total area, on the other hand the area occupied by bare soil decreased by 151 km² or 26.93% of the total area of the study area between 1986 and 2023. It is obvious that due to the rapid development of buildings in the form of residential, commercial, industrial areas, transport networks, sidewalks and parking lots, that buildings are the occupation unit with the greatest expansion while bare soil is the only occupation unit that has declined, this is due to the use of empty land for the construction of all types of infrastructure and in some cases, empty land is transformed into agricultural plots. Concerning the occupation units, vegetation has a lower LST index in 2000 and 2010 with 1°C while water has a lower LST index between 1986 and 2023 by 2 to 10°C. Buildings and bare soil have the highest LST indices. Of the two occupation units, bare soil has a higher LST index ranging from 0.45 to 5°C between 1986 and 2023 The results relating to the relationship between LST and NDVI and between LST and NDBI successively gave negative and positive correlations. For LST and NDVI the correlation is weak for the 4 years 1986, 2000, 2010 and 2023 while the correlation between LST and NDBI is strong for the years 1986, 2000, 2010 and weak for 2023. The analysis showed that the higher the NDVI index, the lower the LST index and the lower the NDVI index, the higher the LST index. Similarly, the higher the NDBI index, the higher the LST index and the lower the NDVI index, the lower the LST index. These relationships demonstrate the effectiveness of vegetation in regulating surface temperatures. These different results encourage us to raise several societal issues and to consider possible solutions related to good planning for the well-being of populations in urban areas. In the immediate future, compliance with building construction standards, a campaign to enhance green spaces in urban areas and to plant trees in open spaces, the enhancement of existing water points and the creation of artificial water points would constitute an important step towards resolving the problems related to urban heat islands. Furthermore, aware of the ecological and energy issues of our time, you will agree with me on the role that surface temperatures could play in optimizing the installation of solar panels and on the influence of vegetation on air pollution.

ACKNOWLEDGEMENTS

We would like to sincerely thank the Centre de Suivi Ecologique (CSE) based in Dakar, Senegal, for its invaluable and ongoing support in this work. Their collaboration was essential to the success of this project. We also thank the National Aeronautics and Space Administration (NASA) and the United States Geological Survey (USGS) for providing free access to satellite data.

References

[1] Oke, T.R., Johnson, G.T., Steyn, D.G. and Watson, I.D (1991). Simulation of surface urban heat islands under 'ideal' conditions at night part 2: Diagnosis of causation. Bound.-Layer Meteorol 56, 339–358.

[2] Lin, P., Lau, S.S.Y., Qin, H. and Gou, Z (2017). Effects of urban planning indicators on urban heat island: a case study of pocket parks in high-rise high-density environment. Landsc. Urban Plan. 168, 48–60.

[3] Alobaydi, D., Bakarman, M.A. and Obeidat, B (2016). The Impact of Urban Form Configuration on the Urban Heat Island: The Case Study of Baghdad, Iraq. Procedia Eng., ICSDEC 2016 – Integrating Data Science, Construction and Sustainability 145, 820–827.

[4] Rosenzweig, C., Solecki, W.., Parshall, L., Chopping, M. and Pope, G (2005). Characterizing the urban heat island in current and future climates in New Jersey. Glob. Environ. Change Part B Environ. Hazards 6, 51–52.

[5] Hu, Y., White, M. and Ding, W (2016). An Urban Form Experiment on Urban Heat Island Effect in high Density Area. Procedia Eng., Fourth International Conference on Countermeasures to Urban Heat Island, 30-31 May and 1 June 2016 169, 166–174.

[6] Kłysik, K. and Fortuniak, K (1999). Temporal and spatial characteristics of the urban heat island of Łód´z, Poland. Atmos. Environ. 33, 3885–3895.

[7] Lemonsu, A., Viguié, V., Daniel, M. and Masson, V (2015). Vulnerability to heat waves: Impact of urban ex- pansion scenarios on urban heat island and heat stress in Paris (France). Urban Clim. 14, Part 4, 586–605.

[8] Stone, B. and Rodgers, M.O (2001). Urban form and thermal effiency: how to design of cities influences the urban heat island. J. Am. Plann. Assoc. 67, 186–198.

[9] Lehoczky, A., Sobrino, J., Skokovic, D., and Aguilar, E (2017). The Urban Heat Island Effect in the City of Valencia: A Case Study for Hot Summer Days. Clim. Change Impacts Adapt. Strateg. Urban Environ. Urban Sci. 2017, 1(1), 9, 2-18.

[10] chatz, J. and Kucharik, C.J (2014). Seasonality of the Urban Heat Island Effect in Madison, Wisconsin. J Appl Meteor Clim. 53, 2371–2386.

[11] Li, X-X. and Norford, L (2016). Evaluation of cool roof and vegetations in mitigating urban heat island in a tropical city, Singapore. Urban climate 16, 59–74.

[12] Tran, H., Uchihama, D., Ochi, S. and Yasuoka, Y (2006). Assessment with satellite data of the urban heat island effects in Asian mega cities. Int. J. Appl. Earth obs. Geoinformation 8, 34–48.

[13] Hassid, S., Santamouris, M., Papanikolaou, N., Linardi, A., Klitsikas, N., Georgakis, C. and Assimakopoulos, D.N (2000). The effect of the Athens heat island on air conditioning load. Energy Build. 32, 131–141.

[14] Li, D. and Bou-Zeid, E (2013). Synergistic Interactions between Urban Heat Islands and Heat Waves: The Impact in Cities Is Larger than the Sum of Its Parts. J. Appl. Meteorol. Climatol. 52, 2051-2064.

[15] Hidalgo, J., Masson, V. and Gimeno, L (2009). Scaling the Daytime Urban Heat Island and Urban-Breeze Circulation. J Appl Meteor Clim. 49, 889-901.

[16] Pinho, O.S. and Orgaz, M.D.M (2000). The urban heat island in a small city in coastal Portugal. Int J Biometeorol 44, 198–203.

[17] Parmentier, Amélie (2010). Élaboration d'un outil d'aide à la décision pour atténuer le phénomène d'îlots de chaleur en milieu urbain. Mémoire de maîtrise électronique, Montréal, École de technologie supérieure, 84p.

[18] Kim, Y.-H. and Baik, J.J (2002). Maximum Urban Heat Island Intensity in Seoul. J Appl Meteor 41, 651–659.

[19] Chow, W.T.L. and Roth, M (2006). Temporal dynamics of the urban heat island of Singapore. Int J Clim. 26, 2243–2260.

[20] Bornstein, R. and Lin, Q (2000). Urban heat islands and summertime convective thunderstorms in Atlanta: three case studies. Atmos. Environ. 34, 507–516.

[21] Li X., Zhou Y., Asrar GR., Imhoff M. and Li, X (2017). The surface urban heat island response to urban expansion. A panel analysis for the conterminous United States. Sci Total Environ. 2017 Dec 15; 605- 606:426-435.

[22] Hinkel, K.M., Nelson, F.E., Klene, A.E. and Bell, J.H (2003). The urban heat island in winter at barrowalaska. Int. J. Climatol. 23, 1889 – 1905.

[23] Weiqi, Z., Yuguo, Q., Xiaoma; L., Weifeng, L. and Lijian, H (2013). Relationships between land cover and the surface urban heat island: seasonal variability and effects of spatial and thematic resolution of land cover data on predicting land surface temperatures. Landscape Ecology, 29(1).

[24] Ivajnši˘c, D., Kaligari˘c, M. and Žiberna, I (2014). Geographically weighted regression of the urban heat island of a small city. Appl. Geogr. 53, 341–353. 24

[25] Peng, S., Piao, S., Ciais, P., Friedlingstein, P., Ottle, C., Bréon, F.-M., Nan, H., Zhou, L., Myneni, R.B (2012). Surface Urban Heat Island Across 419 Global Big Cities. Env. Sci Technol 46, 696–703.

[26] Jinlong, Y., Chaohui, Y., Zihao, A., Bo, M., Qian,W., Yingchao, L., Yali, Z., Weiqiang, C., Ling, W., and Yang, S (2023). The Influence of Urban Form on Land Surface Temperature: A Comprehensive Investigation from 2D Urban Land Use and 3D Buildings Journals Land, 12 (9), 2-18.

[27] Arnfield,J (2003). Two decades of urban climate research: A review of turbulence, exchanges of energy and water, and the urban heat island. International Journal of Climatology, 23, 1–26.

[28] Vasileios,C. D., Anastasia, S., Vasileios,J. G. and George, D (2015). Diachronic land uses changes in semi mountainous areas next to urban and tourist areas. International Journal of Innovative Technology and Exploring Engineering (IJITEE), 4(10), 1-14.

[29] Guifeng,H. and Jianhua, X (2013). Land Surface Phenology and Land Surface Temperature Changes along an Urban–Rural Gradient in Yangtze River Delta, China.Environmental Management, 52(1), 234-49.

[30] Navin, R. and Jonathan, A. F (1999). Estimating historical changes in global land cover: Croplands from 1700 to 1992, Global Biogeochemical Cycles, 13(4), 997-1027.

[31] Braimoh, A.K. and Vlek, P.L.G (2005). Land-Cover Change Trajectories in Northern Ghana. Environmental Management, 36, 356-373.

[32] Liu, J., Curry, J. A., Rossow, W. B., Key, J. R. and Wang, X (2005). Comparison of surface radiative flux data sets over the Arctic Ocean, J. Geophys. Res., 110, 1-13.

[33] N'guessan, E., Dibi, N.H., Bellan, M.F. and Blasco, F (2006). Pression anthropique sur une réserve forestière en Cote d'Ivoire: Apport de la télédétection. Revue Télédétection, 5, 307-323.

[34] Gbombélé, S., Ernest K.A., Emmanuel, K. K., Tanina, D.S., Sékouba O., Mahaman, B.S., Nagnin,S. and Jean, B (2014). Contribution of remonte sensing to the cartography of land use dynamic evolution in the region des Lacs (Centre de la Côte d'Ivoire),Afrique SCIENCE, 10(3), 146 – 160.

[35] Sharma, R., Chakraborty, A. and Joshi, P.K (2015) .Geospatial quantification and analysis of environmental changes in urbanizing city of Kolkata (India). Environ. Monit. Assess, 187(1), 4206 -7.

[36] Estoque, R.C., Murayama, Y. and Myint, S.W (2017). Effects of landscape composition and pattern on land surface temperature: An urban heat island study in the megacities of Southeast Asia. Sci. Total Environ, 577, 349-359.

[37] Ndiaye, M. L.,Traore,V. B., Toure, M. A., Sambou, A., Diaw, A. T and Beye, A. C (2016). Detection and ranking of vulnerable areas to urban flooding using GIS and ASMC (spatial analysis multicriteria): a case study in Dakar, Senegal; International Journal of Advanced Engineering, Management and Science, 2(8), 1270-1277.

[38] Diop, M. and Sagna, P (2012). Vulnérabilité climatique des quartiers de Dakar au Sénégal: Exemple de Nord- Foire-Azur et de Hann-Maristes, Renforcer la resilience au changement climatique des villes: Du diagnostic spatialisé aux mesures d'adaptations (2R2CV), 7 et 8 juillet 2011, Université Paul Verlaine – Mertz, France, Actes du Colloque, 12 p.

[39] Dasylva, S. and Cosandey C (2006).The exploitation of groundwater Quaternary sands for drinking water supply of Dakar offer compromised by inadequate rainfall recharge. Géocarrefour, 80 (4), 349-358.

[40] ANSD, (2013). Situation économique et Sociale régionale, Rapport Avril 2013, 126p.

[41] NDIAYE, M.L (2015) . Détection des changements d'occupation du sol et modélisation géomatique par évaluation multicritère pour la cartographie des zones vulnérables aux inondations dans la région de Dakar/Sénégal. Mémoire de Master, 132p.

[42] Kok, C.T., Hwee, S. L., Mohd, Z.M. and Khiruddin, A (2011). A comparison of radiometric correction techniques in the evaluation of the relationship between LST and NDVI in Landsat imagery, Environmental Monitoring and Assessment 184(6), 3813-29.

[43] Gyanesh,C. and Brian, M (2003) . Revised Landsat-5 TM Radiometric Calibration Procedures and Postcalibration Dynamic Ranges. Geoscience and Remote Sensing, 41 (11), 2674-2677.

[44] Chander, G., Mishra, N., Helder, D. L., Aaron, D. B., Angal, A., Choi, T. et al (2013). Applications of Spectral Band Adjustment Factors (SBAF) for Cross-Calibration. IEEE Transactions on Geoscience and Remote Sensing, 51, 1267-1281.

[45] Belhadj,H. A (2001). Le fonctionnement actuel et passé de sols du Nord Sahara (cuvette de Ouargla). Approches micromorphologique, géochimique et minéralogique et organisation spatiale 198p.

[46] Mostephaoui,M. et Bensaid, R (2014). Caractérisation des sols gypseux dans les zones arides par télédétection : Cas du sous-bassin versant d'oued Djedi-biskra. Lebanese Science Journal, 15(1), 99-115.

[47] Mamadou, A. S (2009). Mapping of changes of land-cover between 1990 and 2002 in the north of Senegal (Ferlo) from Landsat images. European Journal of Geography https://journals.openedition.org/cybergeo/22707.

[48] Escadafal, R., Girard, M.C. and Courault, D (1989). Munsell Soil Color and Reflectance in the Visible Spectral Bands of Landsat MSS and MT Data. Remote Sensing of Environment, 27, 37-46.

[49] Ndéye,Y.B., Mamadou,L.N., Célestin, H. and Bienvenu,S (2019). Using Remote Sensing Technics for Land Use Land Cover Changes Analyses from 1950s to 2000s in Somone Tropical Coastal Lagoon. American Journal of Remote Sensing, 7 (2), 25-34.

[50] Iman,R., Omar, M.S., Rajan,D.G., Haraldur, O., Manjula, R., Yuji, M.H. Z., and Terence, D.M (2018) .Spatiotemporal Analysis of Land Use/Land Cover and Its Effects on Surface Urban Heat Island Using Landsat Data: A Case Study of Metropolitan CityTehran (1988–2018). Sustainability 2018, 10 (4433), 2-25.

[51] Sara, A. G., Mahdi,P., and Fatemeh,R (2013) .The Relationship between NDVI and LST in the urban area of Mashhad, Iran. International Conference on Civil EngineeringArchitecture & Urban Sustainable Development, 27(28), 1-7.

[52] Salah, E. B. B., Wael, E. Z., and Khéloufi, B (2011) .Étude diachronique des changements du couvert végétal dans un écosystème montagneux par télédétection spatiale: cas des monts du Tessala (Algérie occidentale), Physio-Géo, 5 (1), 211-225.

[53] Garouani,E.A. et AHARIK,K. (2021) . Apport des images landsat à l'étude de l'évolution de l'occupation du sol dans la plaine de saïss au maroc, pour la période 1987-2018. Revue Française de Photogrammétrie et de Télédétection, 223(1), 173–188.

[54] Aïssatou, S., Mamadou,A.S., Alioune,K. and Marième,D (2018). L'assèchement des lacs littoraux de la grande côte du Senegal: mythe ou réalité? Cas des lacs Thiourour Warouwaye et Wouye de la banlieue de Dakar. Journal of Animal and Plant Sciences, 35 (2), 5623-5638.

[55] Serigne, M. D (2021) . Étude photogrammétrique de l'infrarouge thermique par drone: intérêt pour l'agriculture de précision 3ème Conférence Internationale sur l'Intensification Durable, 23 au 26 novembre 2021, Dakar,Senegal.

[56] Roy, D.P., Wulder, M.A., Loveland, T.R., et al. (2014) Landsat-8: Science and Product Vision for Terrestrial Global Change Research. Remote Sensing of Environment, 145, 154-172.